Rickettsia parkeri Sca2 promotes dissemination in an intradermal infection mouse model

Thomas P. Burke[1]*, Cuong J. Tran[1,2], Patrik Engström[1], Dustin R. Glasner[2,3], Diego A. Espinosa[2,4], Eva Harris[2], Matthew D. Welch[1]*

[1]Department of Molecular and Cell Biology, University of California, Berkeley, Berkeley, CA, USA

[2]Division of Infectious Disease and Vaccinology, School of Public Health, University of California, Berkeley, Berkeley, CA, USA

[3]Current address: Department of Laboratory Medicine, University of California, San Francisco, San Francisco, CA, USA

[4]Current address: Metagenomi, Emeryville, CA, USA

*email: tburke@berkeley.edu; welch@berkeley.edu

Abstract

Arthropod-borne pathogens cause severe human and animal diseases worldwide; however, current animal models are often inadequate in recapitulating key features of infection. Here, we report an intradermal infection model for *Rickettsia parkeri*, which causes eschar-associated spotted fever rickettsiosis in humans. We show that infection of mice lacking both interferon receptors (*Ifnar*$^{-/-}$*Ifngr*$^{-/-}$) with *R. parkeri* causes skin lesion formation similar to human eschars and disseminated disease with as few as 10 bacteria. Using this model, we found that the actin-based motility protein Sca2 is dispensable for *R. parkeri* survival in organs but is required for *R. parkeri* dissemination from the skin to peripheral tissues and for causing lethal disease. We also found that immunizing mice with *sca2* and *ompB* mutant *R. parkeri* protects against subsequent rechallenge with wild-type bacteria. This study characterizes a mouse model that mimics aspects of human rickettsial disease and reveals a pathogenic role for the *R. parkeri* actin-based motility protein Sca2 in dissemination.

Introduction

Obligate cytosolic bacterial pathogens in the family Rickettsiaceae are a diverse group of arthropod-borne microbes that cause severe human disease worldwide, including spotted fever, scrub typhus, and typhus[1–3]. Many critical aspects of disease caused by obligate cytosolic bacterial pathogens remain unknown, as there are few model pathogens that can be handled under biosafety level 2 (BSL2) conditions with corresponding mouse models that recapitulate key features of human disease[4–6]. One model that has emerged to study the pathogenesis of spotted fever group *Rickettsia* species is *Rickettsia parkeri*, which causes mild eschar-associated spotted fever disease in humans[7]. *R. parkeri* is genetically similar to the more virulent human pathogens *R. rickettsii* and *R. conorii*[8,9], and it can be handled under BSL2 conditions. Moreover, mutants can be generated using transposon mutagenesis[10,11]. However, current mouse models fail to recapitulate symptoms of human disease, limiting investigations into *R. parkeri* pathogenesis.

Small rodents including mice are natural reservoirs for *R. parkeri*[12–15]. However, inbred mice including C57BL/6 and BALB/c develop no or limited skin lesions upon intradermal (i.d.) infection[4]. C3H/HEJ mice, which harbor a mutation in the gene encoding Toll-like receptor 4 (TLR4), the receptor for extracellular lipopolysaccharide (LPS), have been proposed as models for *R. parkeri*, yet they do not develop disseminated disease and only develop minor skin lesions upon i.d. inoculation[4]. C57BL/6 mice have also been proposed as models for *R. parkeri* upon intravenous (i.v.) delivery of 10^8 bacteria[16]. However, this dose is substantially higher than the number of *R. parkeri* found in tick saliva or tick salivary glands[17], and considerable effort is required to generate and concentrate this number of bacteria. An improved mouse model to investigate *R. parkeri* would greatly increase the ability to investigate virulence mechanisms, the host response to infection, human rickettsial disease, and propagation of tick-borne pathogens in animal reservoirs.

One remarkable mechanism of pathogenesis exhibited by cytosolic bacterial pathogens is their ability to manipulate the host cell actin cytoskeleton to propel themselves throughout the cell via actin-based motility. Highly divergent cytosolic bacterial pathogens including *Rickettsia, Listeria, Burkholderia, Mycobacterium,* and *Shigella* species undergo actin-based motility, facilitating cell-to-cell

40 spread[18,19]. Among the factors that mediate actin-based motility, the *L. monocytogenes* actin-based
41 motility factor ActA is one of the best understood. ActA enables *L. monocytogenes* to spread from cell
42 to cell[18,19], escape antimicrobial autophagy[20–23], proliferate in mouse organs after i.v. infection[24,25], and
43 cause lethal disease in mice[26,27]. The pathogenic roles for actin-based motility factors in many other
44 cytosolic bacterial pathogens, however, remain poorly understood. *R. parkeri* actin-based motility differs
45 from that of other pathogens in that it occurs in two phases, one that requires the RickA protein[10,28] and
46 the other that requires the Sca2 protein[10,29]. Only Sca2 is required for efficient cell-to-cell spread *in*
47 *vitro*[10,29], although it is not required for replication in epithelial cells[10,29,30] or avoiding autophagy
48 recognition[31]. Although *sca2* mutant *R. rickettsii* elicit reduced fever in guinea pigs as compared with
49 wild-type (WT) *R. rickettsii*[29], the explanation for reduced fever and the pathogenic role for Sca2 *in vivo*
50 remains unclear. Additionally, Sca2 is not essential for dissemination of *R. parkeri* within the tick
51 vector[32]. Therefore, it remains unresolved how Sca2 enhances rickettsial pathogenesis or fitness.

52 In a recent investigation of the relationship between *R. parkeri* and interferons (IFNs), ubiquitous
53 signaling molecules of the innate immune system that mobilize the cytosol to an antimicrobial state, we
54 observed that mice lacking the genes encoding the receptors for type I interferon (*Ifnar*) and IFN-γ (*Ifngr*)
55 succumb to i.v. infection by *R. parkeri*[33]. Here, we use these IFN receptor-deficient mice to examine the
56 effects of i.d. inoculation of *R. parkeri*, mimicking the natural route of infection. We observe severe skin
57 lesion formation, similar to human infection, as well as disseminated lethal disease with as few as 10
58 bacteria. Using this infection model, we reveal a role for Sca2 in *R. parkeri* dissemination. Finally, we
59 demonstrate that immunization with *sca2* and other mutant *R. parkeri* can protect IFN receptor-deficient
60 mice against subsequent challenge with WT bacteria. This work establishes a mouse model to
61 investigate numerous aspects of *Rickettsia* pathogenesis, including eschar formation, virulence factors,
62 and immunity.

63 **Results**

64 **I.d. infection of *Ifnar*$^{-/-}$*Ifngr*$^{-/-}$ mice causes lethal disease and skin lesions that are grossly similar**
65 **to human eschars.**

66 Although i.v. delivery can recapitulate an immediate systemic disease for many pathogens, it
67 does not mimic the natural route of infection for tick-borne pathogens. In contrast, i.d. delivery better
68 mimics the natural route of infection and allows for investigations into dissemination from the initial
69 infection site to peripheral organs. We therefore sought to develop an i.d. murine infection model to
70 better recapitulate the natural route of tick-borne *R. parkeri* infection. WT, *Tlr4*$^{-/-}$, *Ifnar*$^{-/-}$, *Ifngr*$^{-/-}$, and *Ifnar*
71 $^{-/-}$*Ifngr*$^{-/-}$ C57BL/6J mice, as well as outbred CD-1 mice, were infected i.d. with 10^7 WT *R. parkeri* and
72 monitored over time. No or minor dermal lesions appeared at the site of infection in WT, *Tlr4*$^{-/-}$, *Ifnar*$^{-/-}$,
73 or *Ifngr*$^{-/-}$ C57BL/6J mice or CD-1 mice. In contrast, double mutant *Ifnar*$^{-/-}$*Ifngr*$^{-/-}$ C57BL/6J mice
74 developed large necrotic lesions (**Fig. 1a,b, Extended Data Fig. 1a**) similar to human eschars (**Fig.**
75 **1c**). In some cases, tails of *Ifnar*$^{-/-}$*Ifngr*$^{-/-}$ or *Ifngr*$^{-/-}$ mutant mice became inflamed after i.d. or i.v. infection
76 (**Extended Data Fig. 1b**). These findings demonstrate that interferons redundantly control disease
77 caused by *R. parkeri* in the skin and that i.d. infection of *Ifnar*$^{-/-}$*Ifngr*$^{-/-}$ mice recapitulates the hallmark
78 symptom of human disease caused by *R. parkeri*.

79 Our previous observations using the i.v. route revealed dose-dependent lethality in *Ifnar*$^{-/-}$*Ifngr*$^{-/-}$
80 mice, with 10^7 *R. parkeri* eliciting 100% lethality and 10^5 *R. parkeri* eliciting no lethality[33]. *R. parkeri* are
81 present in tick saliva at a concentration of approximately 10^4 per 1 μl, and approximately 10^7 *R. parkeri*
82 are found in tick salivary glands[17]. However, the number of bacteria delivered from tick infestation likely
83 varies depending on many factors, and we therefore sought to examine the effects of different doses of
84 *R. parkeri* upon i.d. infection of *Ifnar*$^{-/-}$*Ifngr*$^{-/-}$ mice. We observed skin lesion formation at all infectious
85 doses, from 10^7 to 10 bacteria (**Fig. 1d**), suggesting that i.d. infection of *Ifnar*$^{-/-}$*Ifngr*$^{-/-}$ mice elicits lesions
86 with doses similar to what is delivered by tick infestation.

87 We next sought to quantitatively evaluate the effects of i.d. infection by monitoring animal weight,
88 body temperature, the degree of lesion formation, and lethality. Intradermally-infected *Ifnar*$^{-/-}$*Ifngr*$^{-/-}$ mice
89 lost significant body weight (**Fig. 2a; Extended Data Fig. 2a**) and body temperature (**Fig. 2b**; animals

90 were euthanized when body temperature fell below 90° F) as compared with WT mice, whereas infected
91 *Tlr4*$^{-/-}$, *Ifnar*$^{-/-}$, *Ifngr*$^{-/-}$ mice did not. To evaluate lesion severity, we scored lesions upon infection with
92 different doses of *R. parkeri*. Whereas 10^7 bacteria elicited similar responses as 10^5, 10^4, 10^3, and 10^2
93 bacteria (**Fig. 2c**), lesions were less severe when mice were infected with 10^1 bacteria compared with
94 10^7 bacteria. If mice survived, lesions healed over the course of approximately 15-40 days post infection
95 (d.p.i.) at all doses (**Extended Data Fig. 2b**).

96 To investigate whether i.d. infection by *R. parkeri* caused lethal disease, we monitored mouse
97 survival over time. Upon i.d. delivery of 10^7 *R. parkeri,* 8 of 12 *Ifnar*$^{-/-}$*Ifngr*$^{-/-}$ mice exhibited lethargy,
98 paralysis, or body temperatures below 90º F, at which point they were euthanized (**Fig. 1e**), whereas
99 delivery of the same dose of bacteria to WT and single mutant mice did not elicit lesions and all survived
100 (**Fig. 2d**). Lower doses of *R. parkeri* also elicited body weight loss (**Fig. 2a**), body temperature loss
101 (**Extended Data Fig. 2c**), and lethal disease (**Fig. 2d**) in *Ifnar*$^{-/-}$*Ifngr*$^{-/-}$ mice. The cause of lethality in this
102 model remains unclear and will require further investigation. Nevertheless, these findings reveal that
103 i.d. infection can cause lethal disease in *Ifnar*$^{-/-}$*Ifngr*$^{-/-}$ mice with ~10,000-fold lower dose of bacteria than
104 i.v. infection.

105 It remained unclear whether i.d. infection could also be used to model dissemination from the
106 skin to peripheral organs. We therefore evaluated bacterial burdens in spleens and livers of WT and
107 *Ifnar*$^{-/-}$*Ifngr*$^{-/-}$ mice at 5 d.p.i. by measuring *R. parkeri* plaque-forming units (p.f.u.). Bacteria were not
108 recoverable from spleens and livers of intradermally-infected WT mice, suggesting that they did not
109 disseminate from the skin to peripheral organs in high numbers (**Fig. 2e**). In contrast, bacteria were
110 recovered from spleens and livers of intradermally-infected *Ifnar*$^{-/-}$*Ifngr*$^{-/-}$ mice at 5 d.p.i. (**Fig. 2e**). This
111 demonstrates that i.d. infection of *Ifnar*$^{-/-}$*Ifngr*$^{-/-}$ mice with *R. parkeri* causes systemic infection and can
112 be used as a model for dissemination from the skin to peripheral tissues.

113

114 ***R. parkeri* Sca2 is required for lethal disease in *Ifnar*$^{-/-}$*Ifngr*$^{-/-}$ mice.**

115 Sca2 mediates actin-based motility in rickettsial pathogens; however, its contribution to virulence
116 *in vivo* remains unclear. We therefore examined if i.v. and i.d. infections of WT and *Ifnar*$^{-/-}$*Ifngr*$^{-/-}$ mice

117 could reveal a pathogenic role for *R. parkeri* Sca2. Upon i.v. infection with 5 x 10^6 bacteria (**Fig. 3a**) or
118 10^7 bacteria (**Fig. 3b)**, we observed that *sca2*::Tn mutant *R. parkeri* caused reduced lethality compared
119 to WT bacteria. Similarly, i.d. infection with *sca2*::Tn mutant bacteria elicited significantly less lethality
120 (**Fig. 3c**) and weight loss (**Fig. 3d**) as compared to WT bacteria and no severe temperature loss
121 (**Extended Data Fig. 3a**). Although we sought to evaluate infection using a *sca2* complement strain of
122 *R. parkeri,* our attempts to generate such a strain were unsuccessful. As an alternative strategy, we
123 examined whether the transposon insertion itself had an effect on *R. parkeri* survival *in vivo*. We
124 evaluated infection of an *R. parkeri* strain that harbors a transposon insertion in *MC1_RS08740*
125 (previously annotated as *MC1_05535*), which has no known role in virulence[31]. I.v. infection with
126 *MC1_RS08740*::Tn *R. parkeri* caused lethality to a similar degree as WT *R. parkeri* (**Fig. 3a**),
127 demonstrating that the transposon likely does not significantly impact *R. parkeri* fitness *in vivo*.
128 Together, these findings suggest that the actin-based motility factor Sca2 is required for causing lethal
129 disease in *Ifnar*$^{-/-}$*Ifngr*$^{-/-}$ mice.
130

131 **WT and *sca2*::Tn *R. parkeri* elicit similar lesion formation and vascular damage in the skin.**

132 We next examined whether Sca2 facilitates *R. parkeri* dissemination throughout the skin and
133 whether Sca2 is required for lesion formation. Unexpectedly, upon i.d. inoculation, *Ifnar*$^{-/-}$*Ifngr*$^{--}$ mice
134 infected with *sca2*::Tn mutant bacteria developed skin lesions that were of similar severity to lesions
135 caused by WT *R. parkeri*; however, the lesions elicited by *sca2* mutant bacteria appeared significantly
136 earlier than lesions caused by WT bacteria (**Fig. 3e**). Further examinations will be required to better
137 evaluate this observation; however, it may suggest that actin-based motility enables *R. parkeri* to avoid
138 a rapid onset of inflammation in the skin. To evaluate *R. parkeri* dissemination within the skin, we used
139 a fluorescence-based assay that measures vascular damage as a proxy for pathogen dissemination[34].
140 Mice were intradermally infected with WT and *sca2*::Tn *R. parkeri*. At 5 d.p.i., fluorescent dextran was
141 intravenously delivered, and fluorescence was measured at the infection site (**Fig. 3f**, representative
142 small black circle) and in the surrounding area (**Fig. 3f**, representative large black circle). No significant
143 differences were observed when comparing WT and *sca2*::Tn *R. parkeri* infections in *Ifnar*$^{-/-}$*Ifngr*$^{-/-}$ mice

144 using an infectious dose of 10^7 *R. parkeri* in the larger surrounding area (**Fig. 3g**) or at the site of
145 infection (**Extended Data Fig. 4a**). Similar results were observed upon infection with 10^6 or 10^5 bacteria
146 (**Extended Data Fig. 4b,c**). However, significantly more fluorescence was observed in the skin of
147 infected *Ifnar*$^{-/-}$*Ifngr*$^{-/-}$ mice as compared to WT mice (**Fig. 3g**), demonstrating that interferons protect
148 against increased vascular permeability during *R. parkeri* infection. Together, the gross pathological
149 analysis and fluorescence-based assay suggest that Sca2 likely does not significantly enhance *R.*
150 *parkeri* dissemination in the skin during i.d. infection of *Ifnar*$^{-/-}$*Ifngr*$^{-/-}$ mice.
151

152 ***R. parkeri* Sca2 is required for disseminating from the skin to spleens and livers.**

153 We initially hypothesized that *R. parkeri* Sca2 plays a similar pathogenic role *in vivo* to the actin-
154 based motility factor ActA of *L. monocytogenes*, which we found is required for bacterial survival in
155 spleens and livers upon i.v. delivery (**Fig. 3h**), in agreement with previous experiments[24,25]. However,
156 when we examined bacterial burdens upon i.v. infection of *Ifnar*$^{-/-}$*Ifngr*$^{-/-}$ mice with *R. parkeri*, similar
157 amounts of WT and *sca2*::Tn bacteria were recovered in spleens (**Fig. 3i**). We were also surprised to
158 find that significantly more *sca2*::Tn than WT *R. parkeri* were recovered in livers (**Fig. 3i**). The
159 explanation for higher *sca2*::Tn burdens in livers remains unclear. Nevertheless, these data reveal that
160 Sca2 is likely not essential for *R. parkeri* survival in blood, invasion of host cells, or intracellular survival
161 in spleens and livers.

162 We next evaluated the role for Sca2 in *R. parkeri* dissemination by measuring p.f.u. in spleens
163 and livers following i.d. infection of *Ifnar*$^{-/-}$*Ifngr*$^{-/-}$ mice. After i.d. infection, *sca2*::Tn mutant bacteria were
164 ~20-fold reduced in their abundance in spleens and ~2-fold reduced in their abundance in livers as
165 compared to WT *R. parkeri* (**Fig. 3j**). Similar results were seen upon i.d. infection with lower doses of
166 *sca2*::Tn and WT bacteria (**Fig. 3k**). Together, these results suggest that Sca2 is required for *R. parkeri*
167 dissemination from the skin to peripheral tissue.
168

169 ***R. parkeri* actin-based motility does not contribute to avoiding innate immunity *in vitro*.**

170 Sca2-mediated actin-based motility is required for efficient plaque formation and cell-to-cell
171 spread by *R. parkeri in vitro*[10,29]. However, it remains unclear if Sca2 enables *R. parkeri* to escape
172 detection or restriction by innate immunity. The actin-based motility factor ActA enables *L.*
173 *monocytogenes* to avoid autophagy[22,23], and the antimicrobial guanylate binding proteins (GBPs) inhibit
174 *Shigella flexneri* actin-based motility[35]. We therefore sought to evaluate whether Sca2-mediated actin-
175 based motility enables *R. parkeri* to evade innate immunity *in vitro*. We found that the *sca2*::Tn mutant
176 grew similarly to WT bacteria in endothelial cells (**Extended Data Fig. 5a**), consistent with previous
177 reports in epithelial cells[10,29]. We also examined whether Sca2 contributed to *R. parkeri* survival or
178 growth in bone marrow-derived macrophages (BMDMs), which can restrict other *R. parkeri* mutants
179 that grow normally in endothelial cells[31]. However, no significant difference in bacterial survival was
180 observed between WT and *sca2*::Tn bacteria in BMDMs in the presence or absence of IFN-β (**Extended**
181 **Data Fig. 5b**). WT and *sca2* mutant *R. parkeri* also elicited similar amounts of host cell death (**Extended**
182 **Data Fig. 5c**) and IFN-I production (**Extended Data Fig. 5d**). Moreover, we found that the anti-rickettsial
183 factor GBP2 localized to the surface of *sca2*::Tn mutant *R. parkeri* at similar frequency as with WT
184 bacteria in the presence or absence of IFN-β (**Extended Data Fig. 5e,f**). Together, these data suggest
185 that Sca2 does not significantly enhance the ability of *R. parkeri* to evade innate immunity *in vitro*.
186

187 **Immunization with *sca2* and *ompB* mutant *R. parkeri* protects *Ifnar*$^{-/-}$*Ifngr*$^{-/-}$ mice against**
188 **subsequent rechallenge.**

189 We next examined whether *sca2*::Tn mutant *R. parkeri* elicited immunity to subsequent re-
190 challenge with a lethal dose of WT bacteria in *Ifnar*$^{-/-}$*Ifngr*$^{-/-}$ mice. *Ifnar*$^{-/-}$*Ifngr*$^{-/-}$ mice were immunized i.v.
191 with 5 x 10^6 *sca2*::Tn *R. parkeri* and 40 d later were intravenously re-challenged with 10^7 WT *R. parkeri*,
192 which is approximately 10-times a 50% lethal dose (LD_{50})[33]. All mice immunized with *sca2*::Tn *R. parkeri*
193 survived, whereas all naïve mice succumbed by 6 d.p.i. (**Fig. 6a**). We also carried out a similar test with
194 an *R. parkeri* mutant lacking outer membrane protein B (OmpB), which is severely attenuated *in*
195 *vivo*[31,33]. We intravenously infected *Ifnar*$^{-/-}$*Ifngr*$^{-/-}$ mice with 10^7 *ompB* mutant *R. parkeri* and rechallenged
196 them 40 d later with 10^7 WT *R. parkeri*. Mice immunized with *ompB* mutant *R. parkeri* were fully

197 protected from the challenge, whereas naïve mice succumbed by 6 d.p.i. (**Fig. 6a**). Mice immunized
198 with *ompB* and *sca2* mutants also did not lose weight or body temperature upon rechallenge (**Fig. 6b,c**).
199 These data indicate that attenuated *R. parkeri* mutants elicit a robust protective immune response, and
200 that *Ifnar*$^{-/-}$*Ifngr*$^{-/-}$ mice may serve as tools to develop live attenuated *R. parkeri* vaccine candidates.
201

202 **Discussion**

203 In this study, we show that *R. parkeri* infection of *Ifnar*$^{-/-}$*Ifngr*$^{-/-}$ mice via the i.d. route causes
204 eschar formation, a key feature of human disease, and results in dissemination to various organs and
205 in lethality. Using this model, we uncover a role for the *R. parkeri* actin-based motility factor Sca2 in
206 dissemination and in causing lethal disease. We further demonstrate that attenuated *R. parkeri* mutants
207 elicit long-lived immunity. *R. parkeri* is an emerging model to study pathogenesis of obligate cytosolic
208 bacterial pathogens, and the animal model described here will facilitate future investigations into *R.*
209 *parkeri* virulence factors, the host response to infection, the molecular determinants of human disease,
210 and propagation of tick-borne pathogens in wildlife reservoirs.

211 Our study highlights the utility of mouse models that mimic natural routes of infection. Infection
212 via the i.v. and intraperitoneal (i.p.) routes can mimic systemic disease, yet these are unnatural routes
213 for many microbes, including food-borne, arthropod-borne, or aerosol-borne pathogens. Our
214 observation that i.d. infection can cause lethal disease with as few as 10 bacteria (~10,000 fewer
215 bacteria than i.v. infection[33]) suggests that *R. parkeri* may be highly adapted to reside in the skin.
216 Infection of *Ifnar*$^{-/-}$*Ifngr*$^{-/-}$ mice via the i.d. route results in lesion formation similar to human eschars, the
217 hallmark of *R. parkeri* infection, indicating that these mice can serve as models to better understand
218 human disease. *Orientia tsutsugamushi* is the causative agent of scrub typhus[36], a prevalent but poorly
219 understood tropical disease endemic to Southeast Asia[1,37,38]. *O. tsutsugamushi* also causes eschar
220 formation in humans; however, inbred mice do not recapitulate eschar formation during *O.*
221 *tsutsugamushi* infection[5], similar to *R. parkeri* infection. The *Ifnar*$^{-/-}$*Ifngr*$^{-/-}$ model might therefore serve
222 as a tool to investigate the pathogenesis of other arthropod-borne pathogens, including *O.*
223 *tsutsugamushi*. Lastly, saliva from ticks, mosquitos, and sand flies enhances pathogenesis of arthropod-

224 borne bacterial, viral, and parasitic pathogens[39–41], and non-human primates inoculated with *R. parkeri*
225 exhibited altered inflammatory responses when administered after tick-bite[42]. This may suggest a
226 potential role for tick vector components such as tick saliva in *R. parkeri* pathogenesis. Developing
227 improved murine infection models that mimic the natural route of infection, including with the tick vector,
228 is critical to better understand the virulence and transmission of tick-borne pathogens.

229 Many *Rickettsia* species, as well as many facultative cytosolic pathogens including *L.*
230 *monocytogenes*, undergo actin-based motility to spread from cell to cell. For *L. monocytogenes*, the
231 actin-based motility factor ActA enables the pathogen to survive *in vivo*, as *actA* mutant bacteria are
232 over 1,000-fold attenuated by measuring lethality[26,27] and by enumerating bacteria in spleens and livers
233 of mice after i.v. infection[24,25]. However, the pathogenic role for actin-based motility in the Rickettsiae
234 has remained unclear. We find that Sca2 is not required for intracellular survival in organs upon i.v.
235 infection of *Ifnar*$^{-/-}$*Ifngr*$^{-/-}$ mice, but rather, is required for dissemination from skin to peripheral organs
236 and lethality upon i.d. infection. Consistent with an important role for Sca2 in pathogenesis, a previous
237 study reported that i.v. infection of guinea pigs with *sca2* mutant *R. rickettsii* did not elicit fever[29]. Our
238 results suggest that Sca2-mediated actin-based motility by *Rickettsia* may facilitate dissemination
239 through host reservoirs, although we cannot rule out other roles for Sca2 that do not involve actin
240 assembly. *R. prowazekii* and *R. typhi*, which cause severe human disease, encode a fragmented *sca2*
241 gene[43], and undergo no or dramatically reduced frequency of actin-based motility, respectively[44,45].
242 Although it remains unclear why some *Rickettsia* species lost the ability to undergo actin-based motility,
243 Sca2 is dispensable for *R. parkeri* dissemination in the tick vector[32], suggesting that actin-based motility
244 may play a specific role in dissemination within mammalian hosts.

245 We find that *sca2* mutant *R. parkeri*, as well as *ompB* mutant *R. parkeri*, elicit a robust protective
246 immune response in *Ifnar*$^{-/-}$*Ifngr*$^{-/-}$ mice. These findings complement previous observations that *sca2*
247 mutant *R. rickettsii* elicits antibody responses in guinea pigs[29], and expands upon these findings by
248 demonstrating protection from rechallenge and revealing additional vaccine candidates. There are
249 currently limited vaccine candidates that protect against rickettsial disease[6]. Identifying new vaccine
250 candidates may reveal avenues to protect against tick-borne infections and aerosolized *Rickettsia*,

251 which are extremely virulent and potential bioterrorism agents[46], as well as against Brill-Zinsser disease,
252 caused by latent *R. prowazekii*[6]. Future studies exploring whether attenuated *R. parkeri* mutants provide
253 immunity against other *Rickettsia* species are warranted to better define the mechanisms of protection.
254 Finally, we note that these findings on immunity may help develop *R. parkeri* as an antigen delivery
255 platform. *R. parkeri* resides directly in the host cytosol for days and could potentially be engineered to
256 secrete foreign antigens for presentation by major histocompatibility complex I. In summary, the mouse
257 model described here will facilitate future investigations into numerous aspects of *R. parkeri* infection,
258 including actin-based motility and immunity, and may serve as model for other arthropod-borne
259 pathogens.

Figures

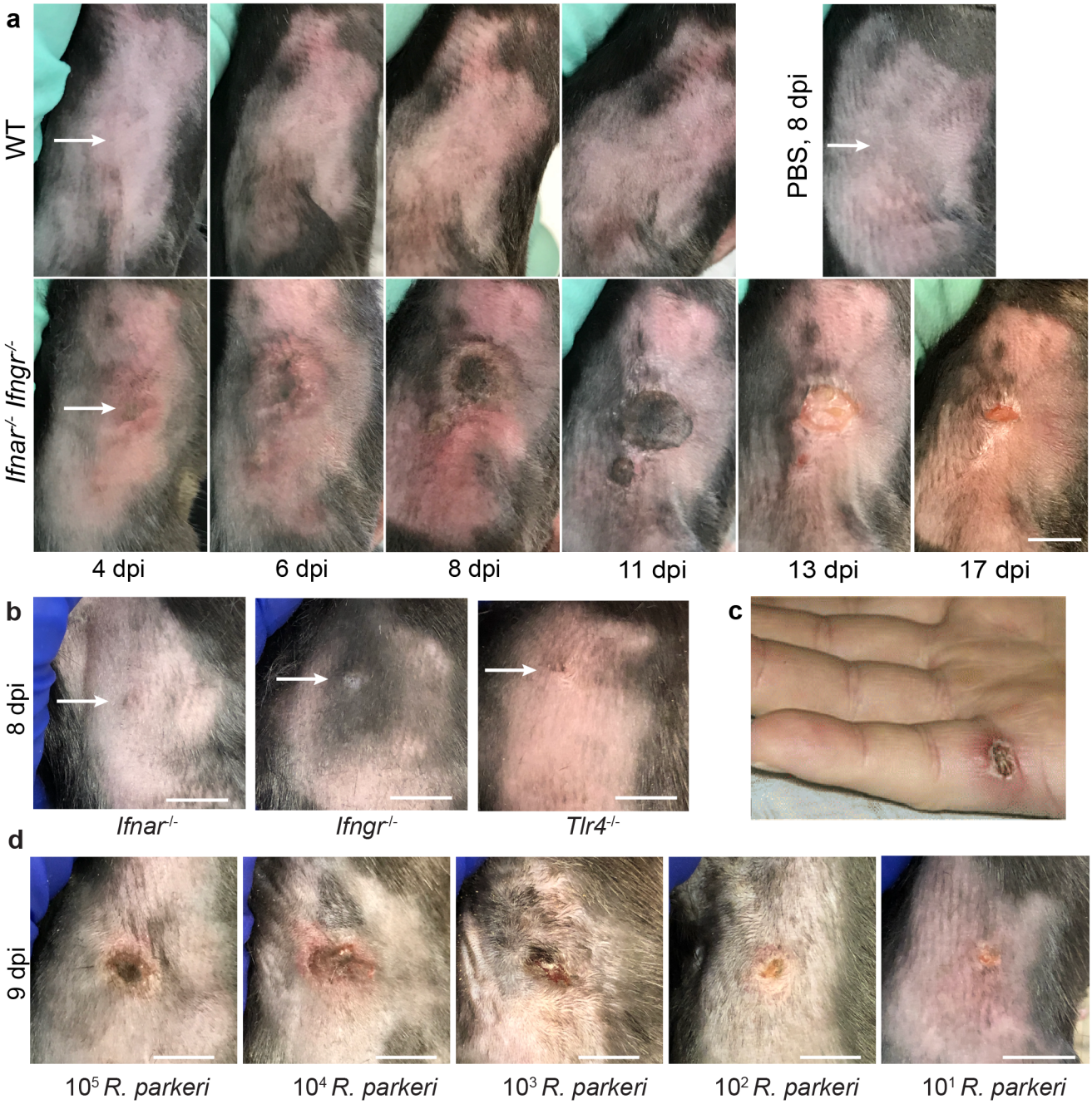

Fig. 1: **I.d. infection of *Ifnar*$^{-/-}$*Ifngr*$^{-/-}$ mice with *R. parkeri* elicits skin lesions that are grossly similar to human eschars.**

a) Representative images of WT and *Ifnar*$^{-/-}$*Ifngr*$^{-/-}$ mice after i.d. inoculation with 10^7 *R. parkeri* (or PBS, in top right image only). Data are representative of 3 independent experiments. White arrows indicate the injection site on the right flank of the mouse. Scale bar, 1 cm. **b**) Representative images of *Ifnar*$^{-/-}$, *Ifngr*$^{-/-}$, and *Tlr4*$^{-/-}$ mice, infected intradermally with 10^7 WT *R. parkeri.* White arrows indicate the infection site on the right flank of the mouse. Scale bar, 1 cm. Data are representative of three independent experiments. **c**) Gross pathology of a human *R. parkeri* infection, from Paddock *et al*[7]. **d**) Representative images of *Ifnar*$^{-/-}$*Ifngr*$^{-/-}$ mice infected intradermally with the indicated amounts of WT *R. parkeri* at 9 d.p.i. Scale bar, 1 cm. Data are representative from two independent experiments.

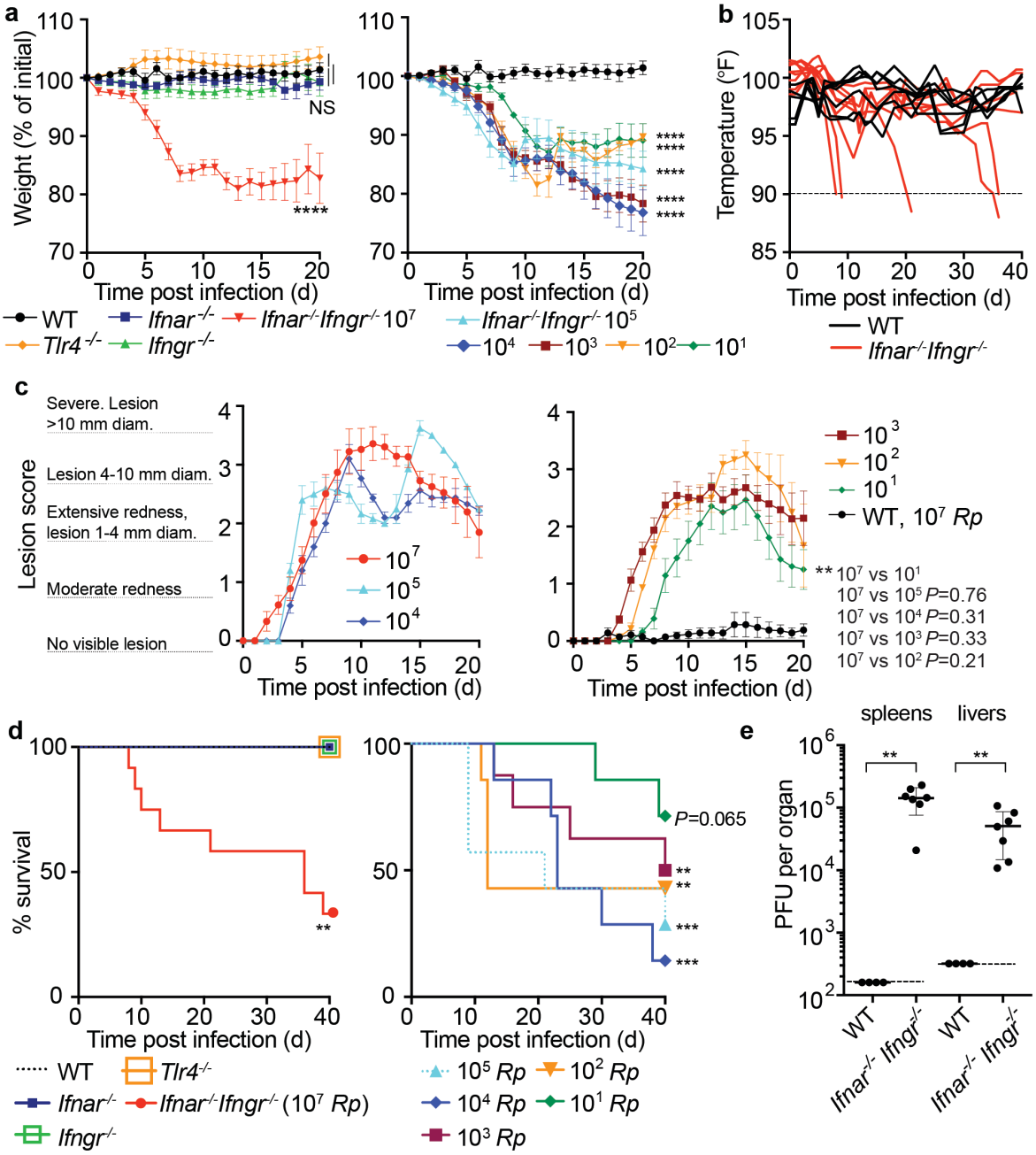

Fig. 2: I.d. infection of *Ifnar*$^{-/-}$*Ifngr*$^{-/-}$ mice by *R. parkeri* elicits disseminated, lethal disease.

a) Weight changes over time in mice infected i.d. with *R. parkeri*. Data are shown as a percentage change to initial weight. In the left panel, all mice were infected with 10^7 *R. parkeri*; *n*=7 (WT), *n*=10 (*Ifnar*$^{-/-}$), *n*=7 (*Ifngr*$^{-/-}$), *n*=9 (*Ifnar*$^{-/-}$*Ifngr*$^{-/-}$) and 4 (*Tlr4*$^{-/-}$) individual mice. In the right panel, *Ifnar*$^{-/-}$*Ifngr*$^{-/-}$ mice were infected with the indicated amounts of *R. parkeri*; *n*=7 (10^5 *R. parkeri*), *n*=7 (10^4 *R. parkeri*), *n*=8 (10^3 *R. parkeri*), *n*=7 (10^2 *R. parkeri*), *n*=7 (10^1 *R. parkeri*) individual mice. WT data is the same in both panels. Data for each genotype are combined from two or three independent experiments. **b**) Temperature changes over time in mice intradermally infected with 10^7 *R. parkeri.* Each line is an individual mouse. Mice were euthanized if their temperature fell below 90° F, as indicated by the dotted line. Data are the combination of three independent experiments with *n*=7 (WT) and 9 (*Ifnar*$^{-/-}$*Ifngr*$^{-/-}$) individual mice. **c**) Analysis of gross skin pathology after i.d. infection. *Ifnar*$^{-/-}$*Ifngr*$^{-/-}$ mice were infected with the indicated number of *R. parkeri* and monitored over time. WT mice were infected with 10^7 *R. parkeri*. Data are the combination of three independent experiments for WT and the 10^7 dose in *Ifnar*$^{-/-}$*Ifngr*$^{-/-}$ mice; data for all other doses are the combination of two independent experiments. *n*=9 (10^7), *n*=5 (10^5), *n*=5 (10^4), *n*=8 (10^3), *n*=7 (10^2), *n*=7 (10^1), and *n*=7 (WT) individual mice. **d**) Mouse survival after i.d. infection with *R. parkeri.* In the left panel, all mice were infected with 10^7 *R. parkeri*; *n*=7 (WT), *n*=11 (*Ifnar*$^{-/-}$), *n*=8 (*Ifngr*$^{-/-}$), *n*=4 *Tlr4*$^{-/-}$, and *n*=12 (*Ifnar*$^{-/-}$*Ifngr*$^{-/-}$) individual mice. Data are the combination of three separate experiments for WT, *Ifnar,* and *Ifnar*$^{-/-}$*Ifngr*$^{-/-}$ and two separate experiments for *Ifngr*$^{-/-}$ and *Tlr4*$^{-/-}$. In the right panel, *Ifnar*$^{-/-}$*Ifngr*$^{-/-}$ mice were infected with the indicated amounts of *R. parkeri.* Data are the combination of two independent experiments; *n*=7 (10^5), *n*=7 (10^4), *n*=8 (10^3), *n*=7 (10^2), and *n*=7 (10^1) individual mice. **e**) Bacterial burdens in organs of intradermally infected WT and *Ifnar*$^{-/-}$*Ifngr*$^{-/-}$ mice. Mice were intradermally inoculated with 10^7 *R. parkeri*, and spleens and livers were harvested and plated for p.f.u. at 72 h.p.i. Dotted lines indicate the limit of detection. Data are the combination of two independent experiments. *n*=4 (WT) and 7 (*Ifnar*$^{-/-}$*Ifngr*$^{-/-}$) individual mice. Data in **a**, **c** are the mean ± SEM. Statistical analyses in **a** used a two-way ANOVA where each group was compared to WT at t=20 d.p.i. Statistical analyses in **c** used a two-way ANOVA at t=20 d.p.i. Statistical analyses in **d** used a log-rank (Mantel-Cox) test to compare *Ifnar*$^{-/-}$ to *Ifnar*$^{-/-}$*Ifngr*$^{-/-}$ at each dose. Statistical analysis in **e** used a two-tailed Mann-Whitney U test. NS, not significant; ***P*<0.01; ****P*<0.001; *****P*<0.0001.

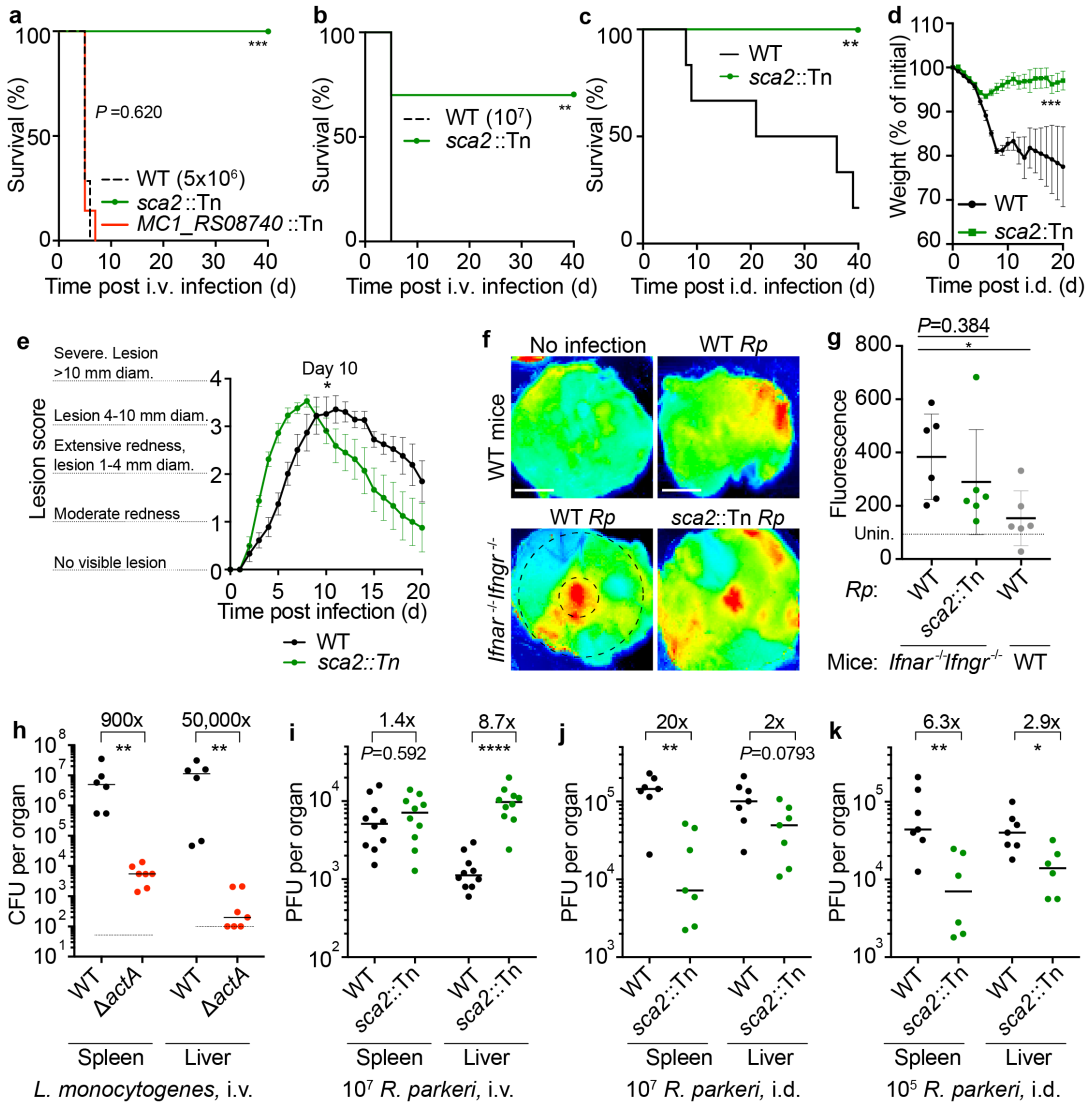

Figure 3: ***R. parkeri* Sca2 contributes to dissemination from skin to peripheral organs.**

a) Survival of *Ifnar*$^{-/-}$*Ifngr*$^{-/-}$ mice upon i.v. infection with 5 x 10^6 *R. parkeri*. *n*=7 (WT), 10 (*sca2*::Tn), and 7 (*MC1_RS08740*::Tn *R. parkeri*) individual mice. Data are the combination of two independent experiments.**b**) Survival of *Ifnar*$^{-/-}$*Ifngr*$^{-/-}$ mice upon i.v. infection with 10^7 *R. parkeri*. *n*=7 (WT) and 10 (*sca2*::Tn) individual mice. Data are the combination of two independent experiments. **c**) Survival of *Ifnar*$^{-/-}$*Ifngr*$^{-/-}$ mice upon i.d. infection with 10^7 *R. parkeri*. *n*=6 (WT) and 8 (*sca2*::Tn) individual mice. Data are the combination of two independent experiments. **d**) Weight changes of *Ifnar*$^{-/-}$*Ifngr*$^{-/-}$ mice upon i.d. infection with 10^7 *R. parkeri*. *n*=6 (WT) and 8 (*sca2*::Tn) individual mice. Data are the combination of two independent experiments. **e**) Analysis of gross skin pathology after i.d. infection. *Ifnar*$^{-/-}$*Ifngr*$^{-/-}$ mice were infected with 10^7 of the indicated strains of *R. parkeri* and monitored over time. *n*=9 (WT) and 8 (*sca2*::Tn) individual mice. Data are the combination of two independent experiments. **f**) Representative images of fluorescence in mouse skin after i.d. infection with 10^6 *R. parkeri* and delivery of a fluorescent dextran, at 5 d.p.i. Scale bars, 1 cm. The larger black dashed circle represents the area that was measured for fluorescence for each sample, as indicated in **Fig. 3g** (~80,000 pixels). The smaller black-dashed circle represents of the injection site area that was measured for fluorescence for each sample, as indicated in **Extended Data Fig. 3** (~7,800 pixels). **g**) Quantification of fluorescence in mouse skin after i.d. infection. Mice were infected with 10^7 *R. parkeri*, and 150 μl fluorescent dextran was intravenously delivered at 5 d.p.i. Skin was harvested 2 h later, and fluorescence was measured using a fluorescence imager. Data indicate measurements of larger areas of skin, as indicated in **f** by the larger black circle. *n*=6 (WT *R. parkeri*) and *n*=6 (*sca2*::Tn *R. parkeri*) individual *Ifnar*$^{-/-}$*Ifngr*$^{-/-}$ mice; *n*=6 (WT *R. parkeri*) individual WT mice. For each experiment, the average of uninfected samples was normalized to 100; each sample was divided by the average for uninfected mice and multiplied by 100; the dotted horizontal line indicates 100 arbitrary units, corresponding to uninfected (unin.) mice. Data are the combination of two independent experiments. **h**) Quantification of *L. monocytogenes* abundance in organs of WT C57BL/6J mice upon i.v. infection with 10^4 bacteria, at 72 h.p.i. Data are the combination of two independent experiments. n=6 (WT), n=7 (Δ*actA*) individual mice. **i**) Quantification of *R. parkeri* abundance in spleens and livers of WT C57BL/6J mice upon i.v. infection, at 72 h.p.i. Data are the combination of two independent experiments. *n*=10 (WT) and 10 (*Sca2*::Tn) individual mice. **j**) Quantification of *R. parkeri* abundance in organs upon i.d. infection with 10^7 *R. parkeri*. *n*=7 (WT) and 7 (*sca2*::Tn) individual mice. Data are the combination of two independent experiments. Data for WT *R. parkeri* in *Ifnar*$^{-/-}$*Ifngr*$^{-/-}$ mice are the same as in **Fig. 2e**. **k**) Quantification of *R. parkeri* abundance in organs upon i.d. infection with 10^5 *R. parkeri*. *n*=7 (WT) and 6 (*sca2*::Tn). Data are the combination of two independent experiments. Solid horizontal bars in **g** indicate means; solid horizontal bars in **h-k** indicate medians; error bars indicate SD. Statistical analyses for survival in **a, b, c** used a log-rank (Mantel-Cox) test. Statistical analysis in **d** used a two-way ANOVA at t=20. Statistical analysis in **e** used a two-way ANOVA from 0 to 10 d.p.i. Statistical analyses in **g** used a two-tailed Student's T test. Statistical analyses in **h, i, j, k** used a two-tailed Mann-Whitney U test. The fold change in **h, i, j, k** indicates differences of medians. **P*<0.05; ***P*<0.01; ****P*<0.001; *****P*<0.0001.

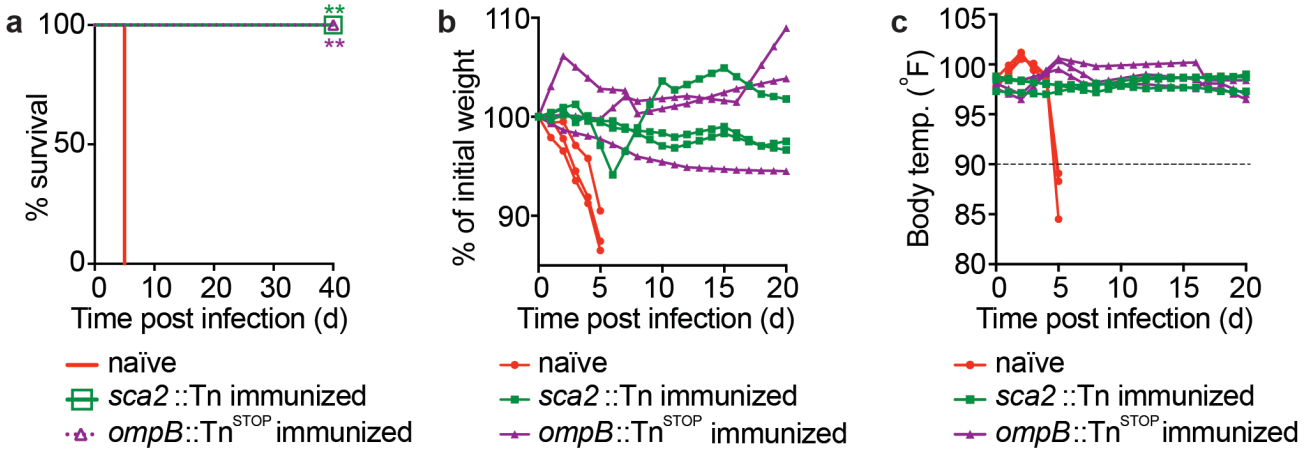

Figure 4: *ompB* and *sca2* mutant *R. parkeri* elicit immunity in *Ifnar*$^{-/-}$*Ifngr*$^{-/-}$ mice.

a) Survival of immunized and naïve *Ifnar*$^{-/-}$*Ifngr*$^{-/-}$ mice upon i.v. *R. parkeri* infection. Immunized mice were first infected with 5x10^{6} *sca2*::Tn or 10^{7} *ompB*:Tn^{STOP} *R. parkeri* and were re-challenged 40 d later with 10^{7} WT *R. parkeri*. *n*=6 (naïve); *n*=5 (*sca2*::Tn immunized); *n*=5 (*ompB*::Tn^{STOP} immunized) individual mice. Data are the combination of two independent experiments.

b) Weight changes over time in mice infected i.d. with 10^{7} *R. parkeri*. Data are representative of two independent experiments. *n*=3 (naïve); *n*=3 (*sca2*::Tn immunized); *n*=3 (*ompB*::Tn^{stop} immunized) individual mice. Each line represents an individual mouse.

c) Temperature changes over time in mice infected i.d. with 10^{7} *R. parkeri.* Data are representative from two independent experiments. *n*=3 (naïve); *n*=3 (*sca2*::Tn immunized); *n*=3 (*ompB*::Tn^{STOP} immunized) individual mice. Each line represents an individual mouse. Statistical analyses in **a** used a log-rank (Mantel-Cox) test to compare each group of immunized mice to naïve mice. ***P*<0.01.

Extended Data Figures

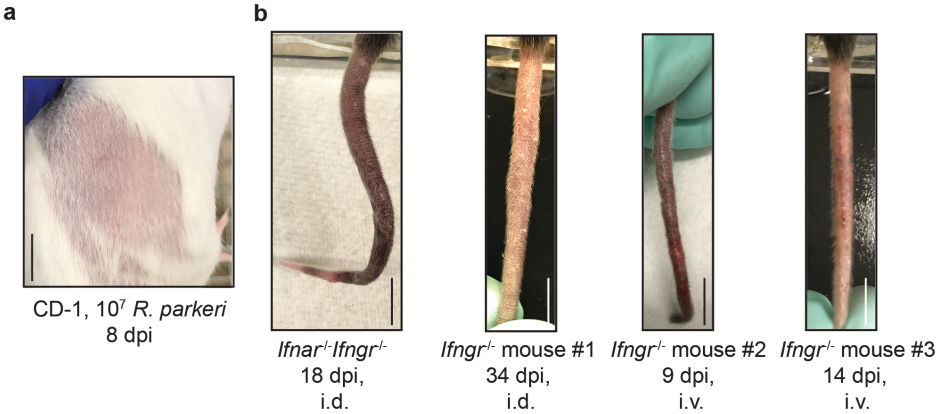

Extended Data Fig. 1: *Ifnar*$^{-/-}$*Ifngr*$^{-/-}$ mice develop disseminated disease upon intradermal *R. parkeri* infection.
a) Representative image of the right flank of CD-1 mice intradermally infected with 10^7 *R. parkeri*. Scale bar, 1 cm. Data are representative from two independent experiments.
b) Representative images of tails of *Ifnar*$^{-/-}$*Ifngr*$^{-/-}$ and *Ifngr*$^{-/-}$ mice, infected via the i.v. or i.d. route (as indicated), with 10^7 WT *R. parkeri.* Some *Ifnar*$^{-/-}$*Ifngr*$^{-/-}$ and *Ifngr*$^{-/-}$ mice had no gross pathological symptoms in the tail, whereas some mice exhibited inflamed, necrotic tails at various times post infection. Scale bar, 1 cm. Data are representative from three independent experiments.

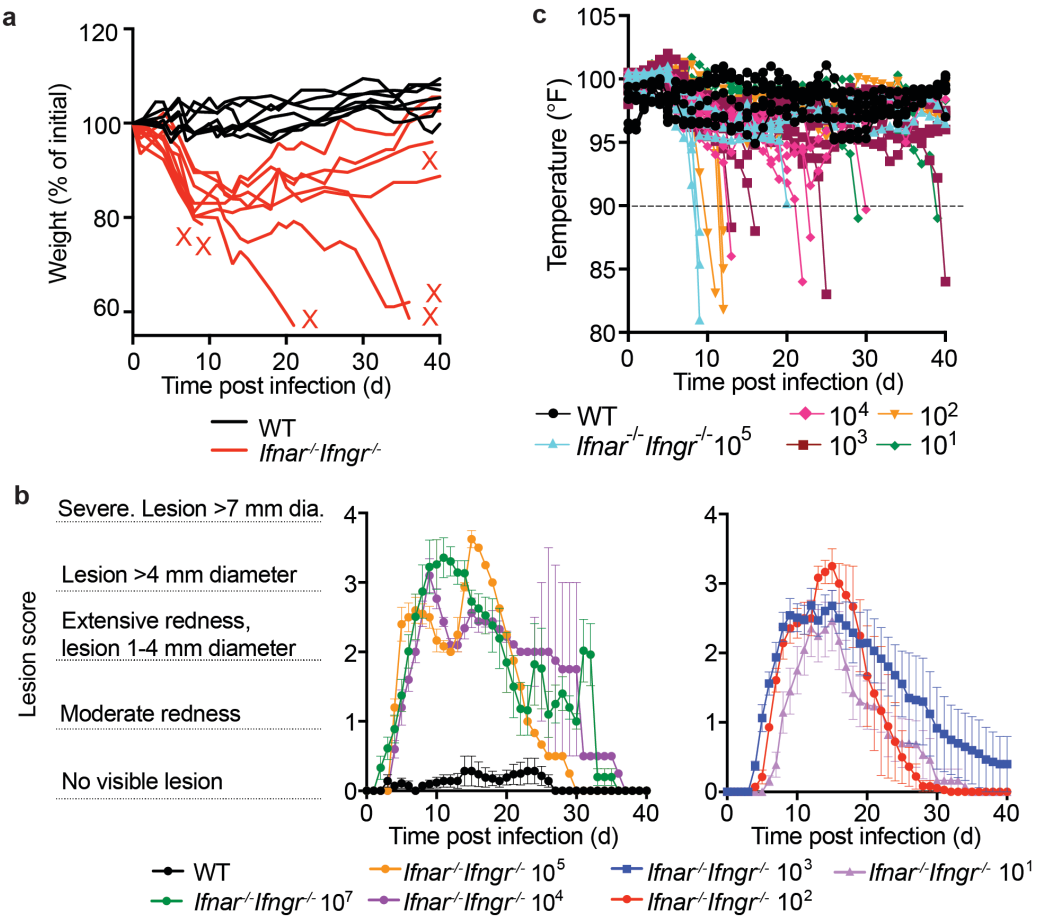

Extended Data Fig. 2: *Ifnar*$^{-/-}$ or *Ifngr*$^{-/-}$ mice develop limited disease upon intradermal infection, and *Ifnar*$^{-/-}$*Ifngr*$^{-/-}$ develop lesions of dose-dependent severity.

a) Weight changes over time in mice intradermally infected with 10^7 WT *R. parkeri*. Data are the combination of two independent experiments for WT and three for *Ifnar*$^{-/-}$*Ifngr*$^{-/-}$; *n*=7 (WT) and *n*=9 (*Ifnar*$^{-/-}$*Ifngr*$^{-/-}$) individual mice. Each line is an individual mouse.

b) Gross pathological analysis of the skin infection site after i.d. infection. *Ifnar*$^{-/-}$*Ifngr*$^{-/-}$ mice were infected with the indicated number of *R. parkeri* and monitored over time. Data are the combination of three independent experiments for the 10^7 dose and two independent experiments for all other doses. *n*=7 (WT), *n*=9 (10^7), *n*=5 (10^5), *n*=5 (10^4), *n*=8 (10^3), *n*=7 (10^2), and *n*=7 (10^1) individual mice. Data are the same as in **Fig. 2c** but are extended to 40 d.p.i.

c) Temperature changes over time in mice infected i.d. with the indicated amounts of WT *R. parkeri.* Data are the combination of two independent experiments; *n*=7 (WT), *n*=7 (10^5), *n*=7 (10^4), *n*=8 (10^3), *n*=7 (10^2), and *n*=7 (10^1) individual mice. Each bar represents an individual mouse. Mice were euthanized if their body temperature fell below 90° F, as indicated by the dotted line.

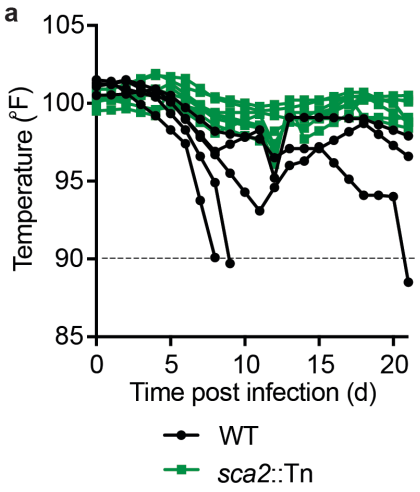

Extended Data Fig. 3: Intradermal infection of *Ifnar*$^{-/-}$*Ifngr*$^{-/-}$ mice with *sca2*::Tn *R. parkeri* causes less severe temperature loss as compared to WT bacteria.
a) Temperature changes over time in mice infected i.d. with 10^7 *R. parkeri.* Data are the combination of two independent experiments; *n*=5 (WT), *n*=8 (*sca2*::Tn) individual mice. Each line represents an individual mouse. Mice were euthanized if their body temperature fell below 90° F, as indicated by the dotted line.

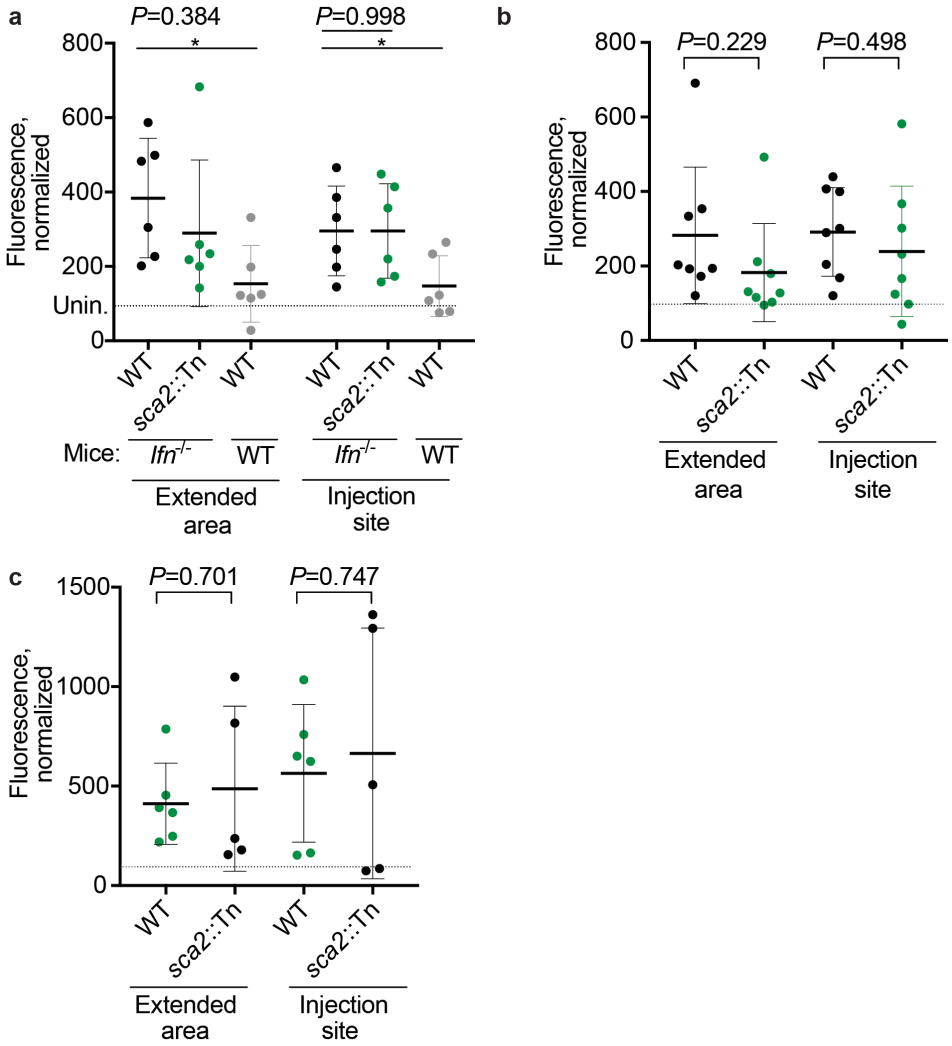

Extended Data Fig. 4: WT and *sca2*::Tn *R. parkeri* elicit similar amounts of vascular damage in skin upon i.d. infection of *Ifnar*$^{-/-}$*Ifngr*$^{-/-}$ mice.

a) Quantification of fluorescence in mouse skin after i.d. infection. Mice were infected i.d. with 10^7 *R. parkeri* and fluorescent dextran was intravenously delivered at 5 d.p.i. Skin was harvested 2 h after delivery of dextran and analyzed with a fluorescence imager. *n*=6 (WT *R. parkeri*) and *n*=6 (*sca2*::Tn *R. parkeri*) individual *Ifnar*$^{-/-}$*Ifngr*$^{-/-}$ mice; *n*=6 (WT *R. parkeri*) individual WT mice. Data in the 'extended area' are the same as those reported in **Fig. 3e**. **b**) Quantification of fluorescence in mouse skin after i.d. infection. Mice were infected i.d. with 10^6 *R. parkeri*, and fluorescent dextran was intravenously delivered at 5 d.p.i. Skin was harvested 2 h after delivery of dextran and analyzed with a fluorescence imager. *n*=8 (WT *R. parkeri*) and *n*=8 (*sca2*::Tn *R. parkeri*) individual *Ifnar*$^{-/-}$*Ifngr*$^{-/-}$ mice. **c**) Quantification of fluorescence in mouse skin after i.d. infection. Mice were infected i.d. with 10^5 *R. parkeri* and fluorescent dextran was intravenously delivered at 5 d.p.i. Skin was harvested 2 h after delivery of dextran and analyzed with a fluorescence imager. *n*=6 (WT *R. parkeri*) and *n*=5 (*sca2*::Tn *R. parkeri*) individual *Ifnar*$^{-/-}$*Ifngr*$^{-/-}$ mice. For each experiment, the average of uninfected samples was normalized to 100, and each sample was divided by the average for uninfected mice and multiplied by 100; the dotted horizontal line indicates 100 arbitrary units, corresponding to uninfected (unin.) mice. Representative sizes for the larger 'extended areas' of skin and the smaller 'injection site' areas of skin are indicated in **Fig. 3d**. Data in **a-c** are each the combination of two independent experiments. Solid horizontal bars indicate means; error bars indicate SD. For statistical analyses, a two-tailed Student's T test was used to compare the indicated samples.

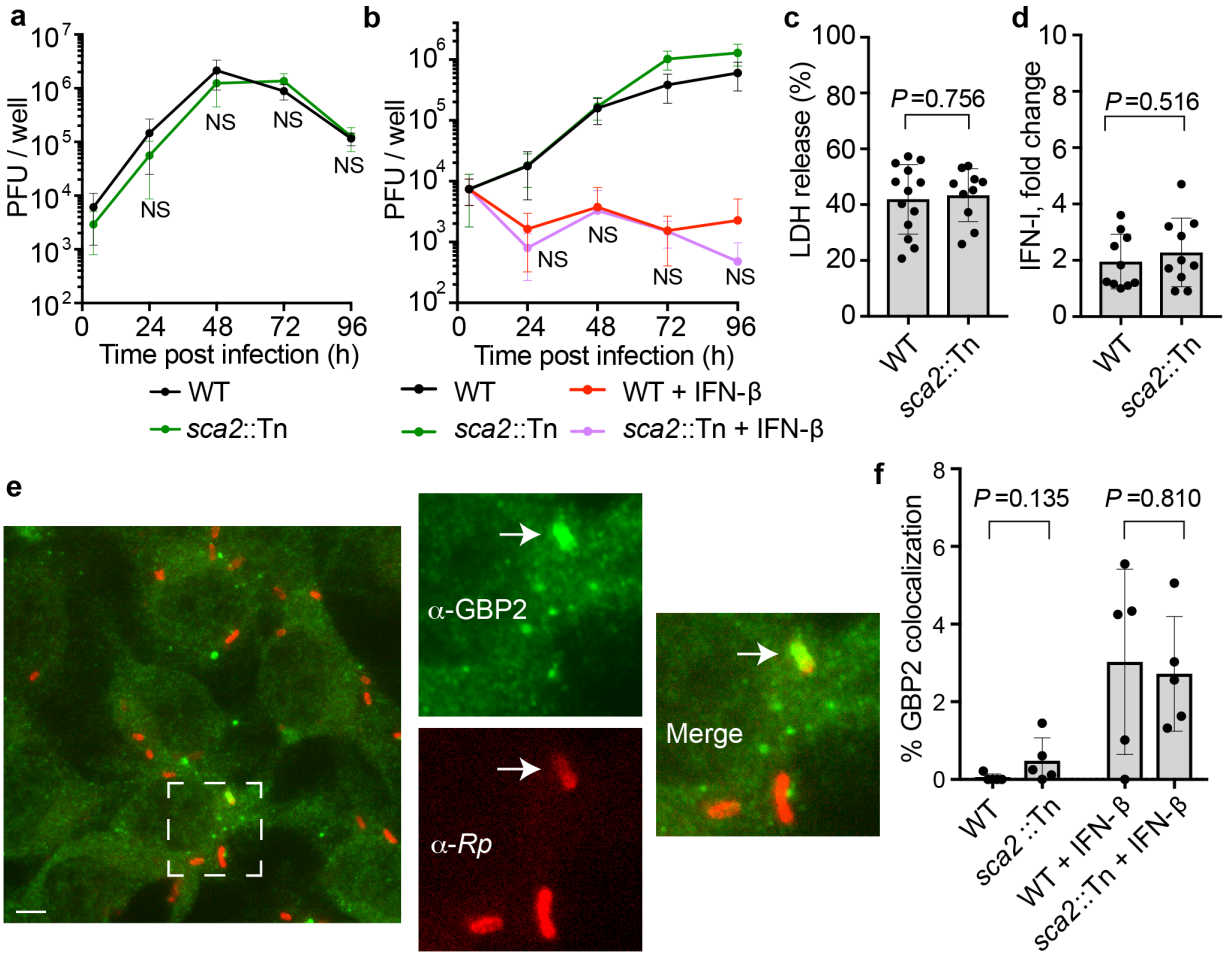

Extended Data Fig. 5: Sca2 does not significantly enhance *R. parkeri* avoidance of antibacterial innate immune responses *in vitro*.

a) *R. parkeri* abundance in HMEC-1s, multiplicity of infection (MOI) of 0.2. Data are the combination of three independent experiments, each with two biological replicates. For statistics, a two-tailed Student's T test was used to compare WT to *sca2*::Tn at 48, 72, and 96 h.p.i. No statistically significant differences were observed at any time. **b**) *R. parkeri* abundance in BMDMs, MOI of 1. Data are the combination of three independent experiments, each with two biological replicates. Data were normalized by multiplying fold difference between WT and *Sca2*::Tn at 4 h.p.i. to *Sca2*::Tn and *Sca2*::Tn + IFN-I data at all time points.**c**) Host cell death upon *R. parkeri* infection of BMDMs, as measured by lactate dehydrogenase (LDH) release assay, MOI of 1. From left to right, *n*=6 and 3 biological replicates and are the combination of two independent experiments. **d**) IFN-I abundance in supernatants of infected BMDMs (24 h.p.i.; MOI of 1), measured using a luciferase reporter assay. The data show the fold change over uninfected cells. *n*=7 and 7 biological replicates and are the combination of two independent experiments. **e**) A representative image using x100 confocal immunofluorescence microscopy of WT BMDMs infected with *sca2*::Tn *R. parkeri* in the presence of 100 U recombinant IFN-β (3 h.p.i.; MOI of 1). Green, α-GBP2; red, α-*Rickettsia* (*Rp*). The dotted square indicates the image that is expanded in the other images, separated into two individual and one merged channel. Scale bars, 2.5 µm. White arrows indicate a bacterium that colocalizes with GBP2. Data are representative of three independent experiments. **f**) Quantification of GBP2 colocalization with *R. parkeri* in BMDMs at 24 h.p.i. Each data point is an average of at least five separate images totaling >150 bacteria. Data are the combination of three independent experiments. Statistical analyses used a two-tailed Student's T test. NS, not significant. Data in **a**,**b** are means; bars in **c**, **d**, and **f** are means; error bars indicate SD.

418 **Methods**
419
420 **Bacterial preparations**
421 *R. parkeri* strain Portsmouth was originally obtained from Dr. Christopher Paddock (Centers for
422 Disease Control and Prevention). To amplify *R. parkeri*, confluent monolayers of female African green
423 monkey kidney epithelial Vero cells (obtained from UC Berkeley Cell Culture Facility, tested for
424 mycoplasma contamination, and authenticated by mass spectrometry) were infected with 5 x 10^6 *R.*
425 *parkeri* per T175 flask. Vero cells were grown in DMEM (Gibco 11965-092) containing 4.5 gl^{-1} glucose
426 and 2% fetal bovine serum (FBS; GemCell). Infected cells were scraped and collected at 5 or 6 d.p.i.
427 when ~90% of cells were rounded due to infection. Scraped cells were then centrifuged at 12,000*g* for
428 20 min at 4˚C. Pelleted cells were resuspended in K-36 buffer (0.05 M KH_2PO_4, 0.05 M K_2HPO_4, 100
429 mM KCl, 15 mM NaCl, pH 7) and dounced for ~40 strokes at 4˚C. The suspension was then centrifuged
430 at 200*g* for 5 min at 4˚C to pellet host cell debris. Supernatant containing *R. parkeri* was overlaid on a
431 30% MD-76R (Merry X-Ray) gradient solution in ultracentrifuge tubes (Beckman/Coulter Cat 344058).
432 Gradients were centrifuged at 18,000 r.p.m. in an SW-28 ultracentrifuge swinging bucket rotor
433 (Beckman/Coulter) for 20 min at 4˚C. These '30% prep' bacterial pellets were resuspended in brain
434 heart infusion (BHI) media (BD, 237500), aliquoted, and stored at -80˚C. Titers were determined by
435 plaque assays by serially diluting the *R. parkeri* in 6-well plates containing confluent Vero cells. Plates
436 were spun for 5 min at 300*g* in an Eppendorf 5810R centrifuge and at 24 h post infection (h.p.i.); the
437 media from each well was aspirated, and the wells were overlaid with 4 ml/well DMEM with 5% FBS
438 and 0.7% agarose (Invitrogen, 16500-500). At 6 d.p.i., an overlay of 0.7% agarose in DMEM containing
439 2.5% neutral red (Sigma, N6264) was added. Plaques were then counted 24 h later. For infections with
440 *ompB* mutant bacteria, the *ompB*^{STOP}::Tn mutant was used, which contains a transposon and an
441 upstream stop codon in *ompB,* as previously described[31].
442
443 **Deriving bone marrow macrophages**
444 For obtaining bone marrow, male or female mice were euthanized, and femurs, tibias, and
445 fibulas were excised. Bones were sterilized with 70% ethanol and washed with BMDM media (20% FBS
446 (HyClone), 0.1% β-mercaptoethanol, 1% sodium pyruvate, 10% conditioned supernatant from 3T3
447 fibroblasts, in DMEM (Gibco) with 4.5 gl^{-1} glucose and 100 µg/ml streptomycin and 100 U/ml penicillin),
448 and ground with a mortar and pestle. Bone homogenate was passed through a 70 µm nylon cell strainer
449 (Thermo Fisher Scientific, 08-771-2) for particulate removal. Filtrates were then centrifuged at 290*g* in
450 an Eppendorf 5810R centrifuge for 8 min, supernatant was aspirated, and the pellet was resuspended
451 in BMDM media. Cells were plated in 30 ml BMDM media in non-TC-treated 15 cm petri dishes at a
452 ratio of 10 dishes per 2 femurs/tibias and incubated at 37˚ C. An additional 30 ml of BMDM media was
453 added 3 d later. At 7 d the media was aspirated, 15 ml cold PBS (Gibco, 10010-023) was added, and
454 cells were incubated at 4˚C with for 10 min. BMDMs were scraped from the plate, collected in a 50 ml
455 conical tube, and centrifuged at 290*g* for 5 min. PBS was aspirated, and cells were resuspended in
456 BMDM media with 30% FBS and 10% DMSO at 10^7 cells/ml. 1 ml aliquots were stored at -80° C for 24
457 h in Styrofoam boxes and then moved to long-term storage in liquid nitrogen.
458
459 **Infections *in vitro***
460 HMEC-1 cells (obtained from the UC Berkeley Cell Culture Facility and authenticated by short-
461 tandem-repeat analysis) were passaged 2-3 times weekly and grown at 37° C with 5% CO_2 in DMEM
462 containing 10 mM L-glutamine (Sigma, M8537), supplemented with 10% heat-inactivated FBS
463 (HyClone), 1 µg/mL hydrocortisone (Spectrum Chemical, CO137), 10 ng/mL epidermal growth factor
464 (Thermo Fisher Scientific, CB40001; Corning cat. no. 354001), and 1.18 mg/mL sodium bicarbonate.
465 HMEC media was prepared every 1-2 months, and aliquoted and stored at 4°C. To prepare HMEC-1
466 cells for infection, cells were treated with 0.25% trypsin-EDTA (Thermo Fisher Scientific); the number
467 of cells was counted using a hemocytometer (Bright-Line), and 3 x 10^4 cells were plated into 24-well
468 plates 48 h prior to infection.
469 To plate macrophages for infection, BMDM aliquots were thawed on ice, diluted into 9 ml of
470 DMEM, centrifuged at 290*g* for 5 min in an Eppendorf 5810R centrifuge, and the pellet was resuspended
471 in 10 ml BMDM media without antibiotics. 5 x 10^5 cells were plated into 24-well plates. Approximately

472 16 h later, "30% prep" *R. parkeri* were thawed on ice and diluted into fresh BMDM media to either 10^6
473 p.f.u./ml or $2x10^5$ p.f.u./ml. Media was then aspirated from the BMDMs, replaced with 500 µl media
474 containing *R. parkeri,* and plates were spun at 300*g* for 5 min in an Eppendorf 5810R centrifuge.
475 Infected cells were incubated in a humidified CEDCO 1600 incubator set to 33˚C and 5% CO_2.
476 Recombinant mouse IFN-β (PBL, 12405-1) was added directly to infected cells after spinfection.
477 For measuring p.f.u., supernatants from infected BMDMs were aspirated, and each well was
478 washed twice with 500 µl sterile milli-Q-grade water. After adding 1 ml of sterile milli-Q water to each
479 well, macrophages were lysed by repeated pipetting. Serial dilutions of lysates were added to confluent
480 Vero cells in 12 well plates. Plates were spun at 300*g* using an Eppendorf 5810R centrifuge for 5 min
481 at room temperature and incubated at 33˚C overnight. At ~16 h.p.i., media was aspirated and replaced
482 with 2 ml/well of DMEM containing 0.7% agarose and 5% FBS (GemCell). At ~6 d.p.i., 1 ml of DMEM
483 containing 0.7% agarose, 1% FBS (GemCell), 200 µg/ml amphotericin B (Invitrogen, 15290-018), and
484 2.5% neutral red (Sigma) was added to each well. Plaques were then counted after 24 h.
485 Microscopy, LDH, and IFN-I experiments were performed as described[33].
486
487 **Animal experiments**
488 Animal research was conducted under a protocol approved by the University of California,
489 Berkeley Institutional Animal Care and Use Committee (IACUC) in compliance with the Animal Welfare
490 Act and other federal statutes relating to animals and experiments using animals (Welch lab animal use
491 protocol AUP-2016-02-8426). The University of California, Berkeley IACUC is fully accredited by the
492 Association for the Assessment and Accreditation of Laboratory Animal Care International and adheres
493 to the principles of the Guide for the Care and use of Laboratory Animals[47]. Mouse infections were
494 performed in a biosafety level 2 facility. All animals were maintained at the University of California,
495 Berkeley campus, and all infections were performed in accordance with the approved protocols. Mice
496 were between 8 and 20 weeks old at the time of initial infection. Mice were selected for experiments
497 based on their availability, regardless of sex. A statistical analysis was not performed to predetermine
498 sample size prior to initial experiments. Initial sample sizes were based on availability of mice and the
499 capacity to process samples within a given time. After the first experiment, a Power Analysis was
500 conducted to determine subsequent group sizes. All mice were of the C57BL/6J background, except
501 for outbred CD-1 mice. All mice were healthy at the time of infection and were housed in microisolator
502 cages and provided chow, water, and bedding. No mice were administered antibiotics or maintained on
503 water with antibiotics. Experimental groups were littermates of the same sex that were randomly
504 assigned to experimental groups. For experiments with mice deficient in *Ifnar* and *Ifngr*, mice were
505 immediately euthanized if they exhibited severe degree of infection, as defined by a core body
506 temperature dropping below 90˚ F or lethargy that prevented normal movement.
507
508 **Mouse genotyping**
509 *Tlr4*$^{-/-}$ [48], *Ifnar*$^{-/-}$ [49], *Ifngr*$^{-/-}$ [50], *Ifnar*$^{-/-}$*Ifngr*$^{-/-}$ and WT C57BL/6J mice were previously described and
510 originally obtained from Jackson Laboratories. CD-1 mice were obtained from Charles River. For
511 genotyping, ear clips were boiled for 15 min in 60 µl of 25 mM NaOH, quenched with 10 µl Tris-HCl pH
512 5.5, and 2 µl of lysate was used for PCR using SapphireAMP (Takara, RR350) and gene-specific
513 primers. Primers used were: *Ifnar* forward (F): CAACATACTACAACGACCAAGTGTG; *Ifnar* WT
514 reverse (R): AACAAACCCCCAAACCCCAG; *Ifnar*$^{-/-}$ R: ATCTGGACGAAGAGCATCAGG; *Ifngr* (F): CTC
515 GTG CTT TAC GGT ATC GC; *Ifngr* (R): TCG CTT TCC AGC TGA TGT ACT; WT *Tlr4* (F):
516 CACCTGATACTTAATGCTGGCTGTAAAAAG; WT *Tlr4* (R):
517 GGTTTAGGCCCCAGAGTTTTGTTCTTCTCA; *Tlr4*$^{-/-}$ (F): TGTTGCCCTTCAGTCACAGAGACTCTG;
518 and *Tlr4*$^{-/-}$ (R): TGTTGGGTCGTTTGTTCGGATCCGTCG.
519
520 **Mouse infections**
521 For mouse infections, *R. parkeri* was prepared by diluting 30%-prep bacteria into cold sterile
522 PBS on ice. Bacterial suspensions were kept on ice during injections. For i.d. infections, mice were
523 anaesthetized with 2.5% isoflurane via inhalation. The right flank of each mouse was shaved with a hair
524 trimmer (Braintree CLP-41590), wiped with 70% ethanol, and 50 µl of bacterial suspension in PBS was
525 injected intradermally using a 30.5-gauge needle. Mice were monitored for ~3 min until they were fully

526 awake. No adverse effects were recorded from anesthesia. For i.v. infections, mice were exposed to a
527 heat lamp while in their cages for approximately 5 min and then each mouse was moved to a mouse
528 restrainer (Braintree, TB-150 STD). The tail was sterilized with 70% ethanol, and 200 µl of bacterial
529 suspension in sterile PBS was injected using 30.5-gauge needles into the lateral tail vein. Body
530 temperatures were monitored using a rodent rectal thermometer (BrainTree Scientific, RET-3).
531 For fluorescent dextran experiments, mice were intravenously injected with 150 µl of 10 kDa
532 dextran conjugated with Alexa Fluor 680 (D34680; Thermo Fisher Scientific) at a concentration of 1
533 mg/ml in sterile PBS[34]. As a negative control, mice with no *R. parkeri* infection were injected with
534 fluorescent dextran. As an additional negative control, uninfected mice were injected intravenously with
535 PBS instead of fluorescent dextran. At 2 h post-injection, mice were euthanized with CO_2 and cervical
536 dislocation, doused with 70% ethanol, and skin surrounding the injection site (approximately 2 cm in
537 each direction) was removed. Connective tissue between the skin and peritoneum was removed, and
538 skin was placed hair-side-up on a 15 cm Petri dish. Skin was imaged with an LI-COR Odyssey CLx (LI-
539 COR Biosciences), and fluorescence was quantified using ImageStudioLite v5.2.5. The skin from mice
540 with no injected fluorescent dextran was used as the background measurement. Skin from mice injected
541 with fluorescent dextran but no *R. parkeri* was normalized to an arbitrary number (100), and *R. parkeri*-
542 infected samples were normalized to this value (*R. parkeri*-infected / uninfected X 100). The number of
543 pixels at the injection site area was maintained across experiments (7,800 for small area and 80,000
544 for the large area).
545 All mice in this study were monitored daily for clinical signs of disease throughout the course of
546 infection, such as hunched posture, lethargy, scruffed fur, paralysis, facial edema, and lesions on the
547 skin of the flank and tail. If any such symptoms were observed, mice were monitored for changes in
548 body weight and temperature. If a mouse displayed severe signs of infection, as defined by a reduction
549 in body temperature below 90˚F or an inability to move normally, the animal was immediately and
550 humanely euthanized using CO_2 followed by cervical dislocation, according to IACUC-approved
551 procedures. Pictures of skin and tail lesions were obtained with permission from the Animal Care and
552 Use Committee Chair and the Office of Laboratory and Animal Care. Pictures were captured with an
553 Apple iPhone 8, software v13.3.1.
554 For harvesting spleens and livers, mice were euthanized at the indicated pre-determined times
555 and doused with ethanol. Mouse organs were extracted and deposited into 50 ml conical tubes
556 containing 4 ml sterile cold PBS for the spleen and 8 ml PBS for the liver. Organs were kept on ice and
557 were homogenized for ~10 s using an immersion homogenizer (Fisher, Polytron PT 2500E) at 22,000
558 r.p.m. Organ homogenates were spun at 290*g* for 5 min to pellet the cell debris (Eppendorf 5810R
559 centrifuge). 20 µl of organ homogenates were then serial diluted into 12-well plates containing confluent
560 Vero cells. The plates were then spun at 260*g* for 5 min at room temperature (Eppendorf 5810R
561 centrifuge) and incubated at 33˚C. To reduce the possibility of contamination, organ homogenates were
562 plated in duplicate and the second replicate was treated with 50 µg/ml carbenicillin (Sigma) and 200
563 µg/ml amphotericin B (Gibco). The next day, at approximately 16 h.p.i., the cells were gently washed
564 by replacing the existing media with 1 ml DMEM containing 2% FBS (GemCell). The media were then
565 aspirated and replaced with 2 ml/well of DMEM containing 0.7% agarose, 5% FBS, and 200 µg/ml
566 amphotericin B. When plaques were visible at 6 d.p.i., 1 ml of DMEM containing 0.7% agarose, 1%
567 FBS, and 2.5% neutral red (Sigma) was added to each well, and plaques were counted at 24 h.p.i.
568
569 **Statistical analysis**
570 Statistical parameters and significance are reported in the figure legends. For comparing two
571 sets of data, a two-tailed Student's T test was performed. For comparing two sets of *in vivo* p.f.u. data,
572 Mann-Whitney *U* tests were used. For comparing two survival curves, log-rank (Mantel-Cox) tests were
573 used. For comparing curves of two samples (mouse health, weight, and temperature), two-way
574 ANOVAs were used. For two-way ANOVAs, if a mouse was euthanized prior to the statistical endpoint,
575 the final value that was recorded for the mouse was repeated until the statistical endpoint. For two-way
576 ANOVAs, if a measurement was not recorded for a timepoint, the difference between values at adjacent
577 time points was used. Data were determined to be statistically significant when $P<0.05$. Asterisks
578 denote statistical significance as: *$P<0.05$; **$P<0.01$; ***$P<0.001$; ****$P<0.0001$, compared to indicated
579 controls. Error bars indicate standard deviation (SD) or, for averages of mouse

health/temperature/weight, standard error of the mean (SEM). All other graphical representations are described in the figure legends. Statistical analyses were performed using GraphPad PRISM v7.0.

Data availability

WT and *ompB* mutant *R. parkeri* were authenticated by whole genome sequencing and are available in the NCBI Trace and Short-Read Archive; Sequence Read Archive (SRA), accession numbers: SRX4401164 (WT) and SRX4401167 (*ompB*::Tn^{STOP}).

Competing interests

The authors declare no competing interests.

Author contributions

T.P.B. performed and analyzed experiments. C.J.T., P.E., D.R.G., and D.A.E. contributed to performing experiments and provided reagents. T.P.B. wrote the original draft of this manuscript with guidance from M.D.W. Critical reading and edits of the manuscript were provided by C.J.T., P.E., and M.D.W. Supervision was provided by T.P.B. and M.D.W.

Acknowledgements

We thank Neil Fisher for editing this manuscript. P.E. was supported by postdoctoral fellowships from the Sweden-America Foundation. M.D.W. was supported by NIH/NIAID grants R01AI109044 and R21AI138550. D.R.G., D.A.E., and E.H. were partially supported by NIH/NIAID grant R01 AI24493 (E.H.).

602 **Bibliography**
603

604 1. Bonell, A., Lubell, Y., Newton, P. N., Crump, J. A. & Paris, D. H. Estimating the burden of scrub
605 typhus: A systematic review. *PLoS Negl. Trop. Dis.* **11**, e0005838 (2017).
606 2. Fang, R., Blanton, L. S. & Walker, D. H. Rickettsiae as Emerging Infectious Agents. *Clinics in*
607 *Laboratory Medicine* **37**, 383–400 (2017).
608 3. Sahni, A., Fang, R., Sahni, S. K. & Walker, D. H. Pathogenesis of Rickettsial Diseases:
609 Pathogenic and Immune Mechanisms of an Endotheliotropic Infection. *Annu. Rev. Pathol.*
610 *Mech. Dis.* **14**, 127–152 (2019).
611 4. Grasperge, B. J. *et al.* Susceptibility of inbred mice to Rickettsia parkeri. *Infect. Immun.* **80**,
612 1846–1852 (2012).
613 5. Sunyakumthorn, P. *et al.* An Intradermal Inoculation Model of Scrub Typhus in Swiss CD-1
614 Mice Demonstrates More Rapid Dissemination of Virulent Strains of Orientia tsutsugamushi.
615 *PLoS One* **8**, (2013).
616 6. Osterloh, A. Immune response against rickettsiae: lessons from murine infection models. *Med.*
617 *Microbiol. Immunol.* **206**, 403–417 (2017).
618 7. Paddock, C. D. *et al.* Rickettsia parkeri Rickettsiosis and Its Clinical Distinction from Rocky
619 Mountain Spotted Fever . *Clin. Infect. Dis.* **47**, 1188–1196 (2008).
620 8. Roux, V. & Raoult, D. Phylogenetic analysis of members of the genus Rickettsia using the gene
621 encoding the outer-membrane protein rOmpB (ompB). *Int. J. Syst. Evol. Microbiol.* **50**, 1449–
622 1455 (2000).
623 9. Goddard, J. Historical and recent evidence for close relationships among Rickettsia parkeri, R.
624 conorii, R. africae, and R. sibirica: Implications for rickettsial taxonomy. *J. Vector Ecol.* **34**, 238–
625 242 (2009).
626 10. Reed, S. C. O., Lamason, R. L., Risca, V. I., Abernathy, E. & Welch, M. D. Rickettsia actin-
627 based motility occurs in distinct phases mediated by different actin nucleators. *Curr. Biol.* **24**,
628 98–103 (2014).
629 11. Lamason, R. L., Kafai, N. M. & Welch, M. D. A streamlined method for transposon mutagenesis
630 of Rickettsia parkeri yields numerous mutations that impact infection. *PLoS One* **13**, 1–12
631 (2018).
632 12. Moraru, G. M. *et al.* Evidence of antibodies to spotted fever group rickettsiae in small mammals
633 and quail from Mississippi. *Vector-Borne Zoonotic Dis.* **13**, 1–5 (2013).
634 13. Moraru, G. M., Goddard, J., Paddock, C. D. & Varela-Stokes, A. Experimental infection of
635 cotton rats and bobwhite quail with Rickettsia parkeri. *Parasites and Vectors* **6**, 1–5 (2013).
636 14. Krawczak, F. S. *et al.* Ecology of a tick-borne spotted fever in southern Brazil. *Exp. Appl.*
637 *Acarol.* **70**, 219–229 (2016).
638 15. Barbieri, A. R. M. *et al.* Species richness and seasonal dynamics of ticks with notes on
639 rickettsial infection in a Natural Park of the Cerrado biome in Brazil. *Ticks Tick. Borne. Dis.* **10**,
640 442–453 (2019).
641 16. Londoño, A. F., Mendell, N. L., Walker, D. H. & Bouyer, D. H. A biosafety level-2 dose-
642 dependent lethal mouse model of spotted fever rickettsiosis: Rickettsia parkeri atlantic
643 rainforest strain. *PLoS Negl. Trop. Dis.* **13**, e0007054 (2019).
644 17. Suwanbongkot, C. *et al.* Spotted fever group rickettsia infection and transmission dynamics in
645 Amblyomma maculatum. *Infect. Immun.* **87**, e00804-18 (2019).
646 18. Choe, J. E. & Welch, M. D. Actin-based motility of bacterial pathogens: mechanistic diversity
647 and its impact on virulence. *Pathog. Dis.* **74**, ftw099 (2016).
648 19. Lamason, R. L. & Welch, M. D. Actin-based motility and cell-to-cell spread of bacterial
649 pathogens. *Current Opinion in Microbiology* **35,** 48–57 (2017).
650 20. Cheng, M. I., Chen, C., Engström, P., Portnoy, D. A. & Mitchell, G. Actin-based motility allows
651 Listeria monocytogenes to avoid autophagy in the macrophage cytosol. *Cell. Microbiol.* **20**,
652 e12854 (2018).
653 21. Mitchell, G. *et al.* Listeria monocytogenes triggers noncanonical autophagy upon phagocytosis,
654 but avoids subsequent growth-restricting xenophagy. *Proc. Natl. Acad. Sci. U. S. A.* **115**, E210–
655 E217 (2017).

22. Yoshikawa, Y. *et al.* Listeria monocytogenes ActA-mediated escape from autophagic recognition. *Nat. Cell Biol.* **11**, 1233–1240 (2009).
23. Yoshikawa, Y., Ogawa, M., Hain, T., Chakraborty, T. & Sasakawa, C. Listeria monocytogenes ActA is a key player in evading autophagic recognition. *Autophagy* **5**, 1220–1221 (2009).
24. Auerbuch, V., Lenz, L. L. & Portnoy, D. A. Development of a competitive index assay to evaluate the virulence of Listeria monocytogenes actA mutants during primary and secondary infection of mice. *Infect. Immun.* **69**, 5953–5957 (2001).
25. Le Monnier, A. *et al.* ActA is required for crossing of the fetoplacental barrier by Listeria monocytogenes. *Infect. Immun.* **75**, 950–957 (2007).
26. Goossens, P. L., Milon, G. & Bevan, M. Induction of protective CD8+ T lymphocytes by an attenuated listeria monocytogenes actA mutant. *Int. Immunol.* **4**, 1413–1418 (1992).
27. Brundage, R. A., Smith, G. A., Camilli, A., Theriot, J. A. & Portnoy, D. A. Expression and phosphorylation of the Listeria monocytogenes actA protein in mammalian cells. *Proc. Natl. Acad. Sci. U. S. A.* **90**, 11890–11894 (1993).
28. Jeng, R. L. *et al.* A Rickettsia WASP-like protein activates the Arp2/3 complex and mediates actin-based motility. *Cell. Microbiol.* **6**, 761–769 (2004).
29. Kleba, B., Clark, T. R., Lutter, E. I., Ellison, D. W. & Hackstadt, T. Disruption of the Rickettsia rickettsii Sca2 autotransporter inhibits actin-based motility. *Infect. Immun.* **78**, 2240–2247 (2010).
30. Haglund, C. M., Choe, J. E., Skau, C. T., Kovar, D. R. & Welch, M. D. Rickettsia Sca2 is a bacterial formin-like mediator of actin-based motility. *Nat. Cell Biol.* **12**, 1057–1063 (2010).
31. Engström, P. *et al.* Evasion of autophagy mediated by Rickettsia surface protein OmpB is critical for virulence. *Nat. Microbiol.* **4**, 2538–2551 (2019).
32. Harris, E. K. *et al.* Role of Sca2 and RickA in the dissemination of Rickettsia parkeri in Amblyomma maculatum. *Infect. Immun.* **86**, e00123-18 (2018).
33. Burke, T. P. *et al.* Inflammasome-mediated antagonism of type I interferon enhances Rickettsia pathogenesis. *Nat. Microbiol.* **5**, 688–696 (2020).
34. Glasner, D. R. *et al.* Dengue virus NS1 cytokine-independent vascular leak is dependent on endothelial glycocalyx components. *PLoS Pathog.* **13**, 1–22 (2017).
35. Piro, A. S. *et al.* Detection of cytosolic shigella flexneri via a C-terminal triple-arginine motif of GBP1 inhibits actin-based motility. *MBio* **8**, e01979-17 (2017).
36. Rajapakse, S., Weeratunga, P., Sivayoganathan, S. & Fernando, S. D. Clinical manifestations of scrub typhus. *Transactions of the Royal Society of Tropical Medicine and Hygiene* **111,** 43–54 (2017).
37. Kelly, D. J., Foley, D. H. & Richards, A. L. A Spatiotemporal Database to Track Human Scrub Typhus Using the VectorMap Application. *PLoS Neglected Tropical Diseases* **9**, e0004161 (2015).
38. Richards, A. L. & Jiang, J. Scrub typhus: Historic perspective and current status of the worldwide presence of Orientia species. *Tropical Medicine and Infectious Disease* **5**, 49 (2020).
39. Pingen, M., Schmid, M. A., Harris, E. & McKimmie, C. S. Mosquito Biting Modulates Skin Response to Virus Infection. *Trends in Parasitology* **33,** 645–657 (2017).
40. Lestinova, T., Rohousova, I., Sima, M., de Oliveira, C. I. & Volf, P. Insights into the sand fly saliva: Blood-feeding and immune interactions between sand flies, hosts, and Leishmania. *PLoS Negl. Trop. Dis.* **11**, e0005600 (2017).
41. Šimo, L., Kazimirova, M., Richardson, J. & Bonnet, S. I. The essential role of tick salivary glands and saliva in tick feeding and pathogen transmission. *Front. Cell. Infect. Microbiol.* **7**, 281 (2017).
42. Banajee, K. H. *et al.* Amblyomma maculatum feeding augments Rickettsia parkeri infection in a rhesus macaque model: A pilot study. *PLoS One* **10**, 1–20 (2015).
43. Ngwamidiba, M., Blanc, G., Ogata, H., Raoult, D. & Fournier, P. E. Phylogenetic study of Rickettsia species using sequences of the autotransporter protein-encoding gene sca2. *Ann. N. Y. Acad. Sci.* **1063**, 94–99 (2005).
44. Teysseire, N., Chiche-Portiche, C. & Raoult, D. Intracellular movements of Rickettsia conorii adn R. typhi based on actin polymerization. *Res. Microbiol.* **143**, 821–829 (1992).

45. Heinzen, R. A., Hayes, S. F., Peacock, M. G. & Hackstadt, T. Directional actin polymerization associated with spotted fever group Rickettsia infection of Vero cells. *Infect. Immun.* **61**, 1926–1935 (1993).
46. Walker, D. H. The realities of biodefense vaccines against Rickettsia. *Vaccine* **27**, D52-55 (2009).
47. National Research Council. *Guide for the Care and Use of Laboratory Animals. The Biochemical journal.* (2010).
48. Hoshino, K. *et al.* Cutting edge: Toll-like receptor 4 (TLR4)-deficient mice are hyporesponsive to lipopolysaccharide: evidence for TLR4 as the Lps gene product. *J. Immunol.* **162**, 3749–52 (1999).
49. Müller, U. *et al.* Functional role of type I and type II interferons in antiviral defense. *Science.* **264**, 1918–1921 (1994).
50. Huang, S. *et al.* Immune response in mice that lack the interferon-γ receptor. *Science.* **259**, 1742–1745 (1993).